HHS Public Access

Author manuscript

Environ Int. Author manuscript; available in PMC 2023 March 01.

Published in final edited form as:

Environ Int. 2023 February ; 172: 107757. doi:10.1016/j.envint.2023.107757.

Triphenyl phosphate-induced pericardial edema in zebrafish embryos is dependent on the ionic strength of exposure media

Jenna Wiegand[a], **Sarah Avila-Barnard**[a], **Charvita Nemarugommula**[a], **David Lyons**[a], **Sharon Zhang**[b], **Heather M. Stapleton**[b], **David C. Volz**[b,*]

[a]Department of Environmental Sciences, University of California, Riverside, CA 92521, United States

[b]Division of Environmental Sciences and Policy, Duke University, Durham, NC 27708, United States

Abstract

Pericardial edema is commonly observed in zebrafish embryo-based chemical toxicity screens, and a mechanism underlying edema may be disruption of embryonic osmoregulation. Therefore, the objective of this study was to identify whether triphenyl phosphate (TPHP) – a widely used aryl phosphate ester-based flame retardant – induces pericardial edema via impacts on osmoregulation within embryonic zebrafish. In addition to an increase in TPHP-induced microridges in the embryonic yolk sac epithelium, an increase in ionic strength of exposure media exacerbated TPHP-induced pericardial edema when embryos were exposed from 24 to 72 h post-fertilization (hpf). However, there was no difference in embryonic sodium concentrations *in situ* within TPHP-exposed embryos relative to embryos exposed to vehicle (0.1% DMSO) from 24 to 72 hpf. Interestingly, increasing the osmolarity of exposure media with mannitol (an osmotic diuretic which mitigates TPHP-induced pericardial edema) and increasing the ionic strength of the exposure media (which exacerbates TPHP-induced pericardial edema) did not affect embryonic doses of TPHP, suggesting that TPHP uptake was not altered under these varying experimental conditions. Overall, our findings suggest that TPHP-induced pericardial edema within zebrafish embryos is dependent on the ionic strength of exposure media, underscoring the importance of further standardization of exposure media and embryo rearing protocols in zebrafish-based chemical toxicity screening assays.

*Corresponding author. david.volz@ucr.edu (D.C. Volz).

CRediT authorship contribution statement

Jenna Wiegand: Conceptualization, Methodology, Validation, Formal analysis, Investigation, Writing – original draft, Writing – review & editing, Visualization. **Sarah Avila-Barnard:** Methodology, Investigation. **Charvita Nemarugommula:** Methodology, Investigation. **David Lyons:** Methodology, Investigation. **Sharon Zhang:** Methodology, Investigation. **Heather M. Stapleton:** Resources, Writing – review & editing, Supervision, Project administration. **David C. Volz:** Conceptualization, Resources, Writing – review & editing, Supervision, Project administration, Funding acquisition.

Declaration of Competing Interest

The authors declare that they have no known competing financial interests or personal relationships that could have appeared to influence the work reported in this paper.

Appendix A. Supplementary data

Supplementary data to this article can be found online at https://doi.org/10.1016/j.envint.2023.107757.

Keywords

Zebrafish; Pericardial edema; Osmoregulation; Triphenyl phosphate; Epithelium

1. Introduction

Pericardial edema – or fluid accumulation surrounding the developing heart – is an abnormal phenotype that is commonly observed across different species of fish embryos following exposure to a wide range of structurally diverse chemicals (Duan et al., 2013; Hermsen et al., 2017; Hill et al., 2004; McCollum et al., 2017; McGruer et al., 2021; Yozzo et al., 2013; Yozzo et al., 2013). Depending on the magnitude and severity, pericardial edema has the potential to interfere with normal developmental landmarks, leading to abnormalities such as cardiac looping defects, bradycardia, and kidney malformations (Hill et al., 2004; Isales et al., 2015; McGee et al., 2012; Mitchell et al., 2019; K.L. Yozzo et al., 2013). In zebrafish embryos, prior studies have suggested that edema may be caused by kidney failure, circulatory failure, ionic imbalance, and permeability defects (Hill et al., 2004). Prior studies have hypothesized that edema may be a stress response that is not linked to any underlying mechanisms, and may be reversed if the severity is low (Brotzmann et al., 2022; Von Hellfeld et al., 2020). The mechanisms underlying edema have been extensively studied within mammalian models and humans but, within the published literature specific to fish, edema is often reported as an abnormal phenotype/endpoint in the absence of mechanistic investigations. Pericardial edema and yolk sac edema are two of the most documented edema phenotypes due to the ability and ease that both endpoints can be measured and analyzed using brightfield microscopy (Narumanchi et al., 2021). Despite the ease of analysis and widespread use of these endpoints, pericardial edema and yolk sac edema are often considered non-specific phenotypes due to the lack of knowledge of underlying mechanisms causing edema formation (Narumanchi et al., 2021).

Zebrafish have emerged as a model teleost species to understand how embryonic and adult fish utilize osmoregulation to maintain homeostasis (Evans, 2011; Fridman, 2020; Pung Hwang et al., 2011; Pung Hwang and Chou, 2013; Kwong et al., 2014). As zebrafish gills continue to develop a capacity for O_2 consumption until approximately 14 d post-fertilization (dpf) (Rombough, 2007), aquaporins and epidermal ionocytes play a critical role in maintaining homeostasis within the developing embryos and larvae (Guh et al., 2015a). Within freshwater species, there are five types of ionocytes – KS (Potassium-Sodium pump), SLC (Sodium, Potassium, Chlorine, Bicarbonate pump), NCC (Sodium, Chlorine, Bicarbonate pump), NaRC (Calcium, Sodium, Potassium pump), and HR (Bicarbonate, sodium, hydrogen, carbon dioxide, ammonia, chlorine pump) (Guh et al., 2015b) – that regulate uptake of potassium, sodium, chlorine, bicarbonate, hydrogen, carbon dioxide and ammonia through aquaporins which, in turn, regulate water exchange between the embryo and surrounding aqueous environment (Kwong and Perry, 2015). Within embryonic zebrafish, the skin is the primary site of osmoregulation prior to gill-specific localization of ionocytes and aquaporins at approximately 14 dpf (Guh et al., 2015a). The skin of embryonic zebrafish also includes keratinocytes with distinct cell borders (Li et al., 2011),

and ionocytes and aquaporins are localized throughout the epidermal layer along these cell borders (Li et al., 2011).

Freshwater fish are dependent on the skin, kidney, intestinal tract, and gills to maintain homeostasis as a result of being constantly surrounded by water that is necessary for survival. The skin serves as a barrier for water and ions, while the kidney excretes water and organic waste (Serluca et al., 2002). Within zebrafish, these systems are critical within early life-stages since embryos rely on oxygen diffusion from the surrounding water in order to survive (Pelster and Burggren, 1996). During development, two separate water permeability barriers – one surrounding the embryonic body and one surrounding the yolk sac (Hagedorn et al., 1998) – allow embryos to regulate water uptake in the absence of a chorion in embryonic zebrafish, albeit the chorion may play a large role in regulating water uptake in other teleosts due to species-specific anatomical differences in the embryonic chorion (Hill et al., 2004). Interestingly, prior studies have demonstrated that impaired maintenance of the barrier surrounding the embryonic body results in edema (Hill et al., 2004). The zebrafish embryonic yolk sac is made up of proteins (mostly vitellogenin) (Ge et al., 2017; Link et al., 2006) and lipids (cholesterol, phosphatidylcholine, and triglycerides), albeit the yolk sac composition is variable across teleost species (Link et al., 2006). The yolk can bioaccumulate toxins from waterborne exposures (Chen et al., 2015; Choi et al., 2016; Dolgova et al., 2016; Souder and Gorelick, 2017), with uptake involving passive or active transport across the yolk sac epithelium (Sant and Timme-Laragy, 2018). The yolk sac epithelium contains a majority of ionocytes found in developing embryos, but there is little information about the function of epidermal ionocytes as well as the susceptibility of epidermal ionocytes to environmental chemicals (Kwong et al., 2016; Sant and Timme-Laragy, 2018). The yolk sac is metabolically active (Cindrova-Davies et al., 2017) and, due to its ability to bioaccumulate hydrophobic environmental chemicals, may alter the normal trajectory of the developing embryo (Sant and Timme-Laragy, 2018).

One of the largest fields that utilizes pericardial edema and yolk sac edema as endpoints within fish embryos is toxicology. One paper compiled all of the studies that utilized zebrafish as a model for toxicology and listed all chemicals that caused abnormal phenotypes, including pericardial edema and yolk sac edema, up to 2011 (Mccollum et al., 2011). At the time of publication, 22 chemicals caused yolk sac edema and 35 chemicals caused pericardial edema within zebrafish embryos, making these the most observed phenotypes (Mccollum et al., 2011). Since 2011, numerous labs around the world have identified a multitude of chemicals that induce pericardial edema and/or yolk sac edema. For example, our recent study found that pericardial edema was associated with elevated epidermal ionocytes within zebrafish embryos following a 24- to 72-hpf exposure to triphenyl phosphate (TPHP), an aryl phosphate ester-based flame retardant and plasticizer (Wiegand et al., 2022). Moreover, we found that co-exposure of embryos to mannitol (an osmotic diuretic) blocked TPHP-induced pericardial edema and effects on ionocyte abundance, whereas knockdown of ATPase1a1.4 – an abundant Na^+/K^+-ATPase localized to epidermal ionocytes – mitigated TPHP-induced effects on ionocyte abundance but not pericardial edema. Overall, our study suggested that TPHP-induced toxicity during early stages of development may potentially be driven by impacts on the osmoregulatory system within embryonic zebrafish (Wiegand et al., 2022).

The objective of this study was to identify whether TPHP impacts osmoregulation within embryonic zebrafish. To accomplish this objective, we first utilized a fluorescent, sodium ion indicator dye and automated image acquisition/analysis protocols to quantify relative sodium concentrations *in situ.* Second, we utilized analytical chemistry to determine if the presence of mannitol or varying ionic strength of the surrounding exposure media affected TPHP uptake into the developing embryo. Third, we relied on ion chromatography and inductively coupled plasma optical emission spectrometry (ICP-OES) to 1) quantify the concentrations of fluoride, chloride, nitrite, bromide, nitrate, phosphate, sulfate, sodium, calcium, potassium, and magnesium in different media used for embryo exposures and 2) determine how varying ion concentrations impacted embryonic phenotypes. Finally, we utilized scanning electron microscopy to determine whether TPHP altered the morphology and/or organization of the yolk sac epithelium, as we previously found that the majority of ATPase1a1-positive ionocytes were localized to the yolk sac epithelium.

2. Materials and methods

2.1. Animals

Using previously described procedures (Mitchell et al., 2018), wild-type adult (strain 5D) zebrafish were maintained and bred on a recirculating system according to an Institutional Animal Care and Use Committee-approved animal use protocol (#20210027) at the University of California, Riverside.

2.2. Chemicals

TPHP (99.5% purity) and D-mannitol (>98% purity) were purchased from ChemService, Inc. (West Chester, PA, USA) and Bio-Techne Corp. (Minneapolis, MN, USA), respectively. To prepare stock solutions, TPHP was dissolved in liquid chromatography-grade dimethyl sulfoxide (DMSO) and stored at room temperature in 2-mL glass amber vials with polytetrafluoroethylene-lined caps. To prepare working solutions, stock solutions of TPHP were spiked into water from our recirculating system (pH and conductivity of ~7–8 and ~900–1000 μS, respectively), resulting in 0.1% DMSO within all vehicle control and TPHP treatments. D-mannitol solutions were freshly prepared by dissolving powder into water from our recirculating system and then immediately used for exposures.

2.3. TPHP exposures

Immediately after spawning, fertilized eggs were collected and incubated in groups of approximately 50 per 100 × 15 mm polystyrene petri dish until 24 h post-fertilization (hpf) within a light- and temperature-controlled incubator. Working solutions of vehicle (0.1% DMSO) or TPHP (2.5 μM, 5 μM, and 10 μM) were prepared as described above. Vehicle or TPHP solutions (10 mL) were added to 100 × 15 mm polystyrene petri dishes and viable embryos were then transferred to dishes, resulting in 30 initial embryos per dish (three replicate dishes per treatment). Embryos were then exposed to vehicle or TPHP from 24 to 72 hpf. All dishes were covered with a lid and incubated under a 14-h:10-h light-dark cycle at 28 °C until 72 hpf. At 72 hpf, embryos were either 1) fixed overnight at 4 °C in 4% paraformaldehyde in 1X phosphate buffered saline (PBS), transferred to 1X PBS, and stored

at 4 °C for no longer than one month until imaging or 2) immediately stained and analyzed for embryonic sodium concentrations as described below.

2.4. Quantification of embryonic sodium concentrations

At 72 hpf, embryos were stained with a fluorescent sodium indicator dye (CoroNa Green AM, Invitrogen, Waltham, MA, USA) to quantify embryonic sodium concentrations *in situ.* At 72 hpf, the embryos were rinsed three times with reverse osmosis (RO) water and then placed in a working solution containing RO water, 20% Pluronic F-127 (Invitrogen, Waltham, MA, USA), and 10 μM CoroNa Green AM for 1.5 h. The working solution was then aspirated, and embryos were washed with RO water three times for 5 min each. Finally, embryos were immobilized with 100 mg/L MS-222 for 3 min, transferred into 96-well plates, and imaged under transmitted light and a FITC filter on our ImageXpress Micro XLS Widefield High-Content Screening System within MetaXpress 6.0.3.1658 (Molecular Devices, Sunnyvale, CA, USA). Body length, pericardial area, and yolk sac area were manually quantified within MetaXpress using images captured under transmitted light, whereas total area of sodium-derived fluorescence in the head, trunk and yolk sac was quantified with a custom module within MetaXpress using images captured under a FITC filter.

2.5. Embryo media experiments

Different concentrations (0.5X, 1X and 2X) of embryo media (EM) were created by diluting a stock concentration of 60X EM within RO water. 60X EM was made in-house by dissolving 17.2 g NaCl, 0.76 g KCl, 2.9 g $CaCl_2{\cdot}2H_20$, and 4.9 g $MgSO_4{\cdot}7H_20$ into 1 L of RO water, and then autoclaving the final solution prior to long-term storage at 4 °C (Brand et al., 2002). Varying concentrations of EM were used for TPHP exposures by spiking DMSO or TPHP into 0.5X, 1X or 2X EM, resulting in a final concentration of either 0.1% DMSO or 5 μM TPHP. Immediately after spawning, fertilized eggs were collected and incubated in groups of approximately 50 per 100 × 15 mm polystyrene petri dish until 24 hpf within a light- and temperature-controlled incubator. Working solutions of vehicle (0.1% DMSO) or 5 μM TPHP in EM (0.5X, 1X or 2X) were prepared as described above. Vehicle or TPHP solutions (10 mL) were added to 100 × 15 mm polystyrene petri dishes and viable embryos were then transferred to dishes, resulting in 30 initial embryos per dish (three replicate dishes per treatment). Embryos were then exposed to vehicle or TPHP from 24 to 72 hpf. All dishes were covered with a lid and incubated under a 14-h:10-h light-dark cycle at 28 °C until 72 hpf. At 72 hpf, all embryos were analyzed as described above.

2.6. EM ingredient experiments

To determine if one of the EM ingredients was necessary for TPHP-induced pericardial edema, exposures of TPHP were performed in four different solutions containing individual ingredients of 2X EM. Four different solutions were prepared in RO water: 10 mM NaCl, 0.17 mM KCl, 0.66 mM $CaCl_2{\cdot}2H_20$, or 0.66 mM $MgSO_4{\cdot}7H_20$. Each of these solutions were then spiked with DMSO or TPHP, resulting in a final concentration of either 0.1% DMSO or 5 μM TPHP. Embryos were then exposed from 24 to 72 hpf as described above. At 72 hpf, all embryos were analyzed as described above.

2.7. Quantification of embryonic doses of TPHP and DPHP

Embryonic doses of TPHP and diphenyl phosphate (DPHP, the primary metabolite of TPHP within mammals) were quantified following exposure to TPHP from 24 to 72 hpf in RO water, system water, or 2X EM as described above. For the first experiment, 24-hpf embryos were transferred to 100 × 15 mm polystyrene petri dishes (30 embryos per dish; four replicate dishes per treatment) containing either system water and 0.1% DMSO, 5 μM TPHP, 250 mM D-Mannitol, or 5 μM TPHP + 250 mM D-Mannitol. For the second experiment, 24-hpf embryos were transferred to 100 × 15 mm polystyrene Petri dishes (30 embryos per dish; four replicate dishes per treatment) containing either 1) RO water + 0.1% DMSO or 5 μM TPHP, or 1) 2X EM + 0.1% DMSO or 5 μM TPHP. All embryos were incubated until 72 hpf. For each replicate group (4 groups per treatment), ~30 embryos were placed into a 2-mL cryovial, immediately snap-frozen in liquid nitrogen, and stored at −80 °C. Prior to extraction, samples were spiked with deuterated TPHP (d15-TPHP) and deuterated DPHP (d10-DPHP). Analytes were extracted and quantified similar to previously published methods (Mitchell et al., 2018). Method detection limits (MDLs) were set as three times the standard deviation of lab blanks. The MDLs for DPHP and TPHP were 0.86 ng and 1.19 ng, respectively, for the first experiment, and 0.05 ng and 0.03 ng, respectively, for the second experiment.

2.8. Ion chromatography and ICP-OES

To determine the concentration of ions within water used in our experiments, 10 mL samples of RO, system water, 0.5X EM, 1X EM, and 2X EM were analyzed within UCR's Environmental Science Research Laboratory. Anions of interest were analyzed using a Dionex AQUION (Sunnyvale, CA) model ion chromatograph (IC) fitted with a conductivity cell detector, a 10-μL sample injection loop, Ion Pac AG14 (4x80 mm), AS14 (4x250 mm) guard and analytical columns maintained at 30 °C, DRS-600 (4 mm) self-regenerating suppressor, and DV40 autosampler. The resin composition was ethylvinylbenzene cross-linked with divinylbenzene. The column specifications were the following: 9-μm particle size, 55% substrate crosslinking, anion exchange capacity of 65 μeq, alkyl quaternary ammonium ion exchange group, and medium-high hydrophobicity. Calibration standards were diluted from certified stock solutions using deionized water prepared via a Labconco WaterPro DS system (Kansas City, MO). Eluent was prepared using this deionized water with the following concentration: 3.5 mM Na_2CO_3/1.0 mM $NaHCO_3$. All glassware was washed using this deionized water. Anions were calibrated using concentrations ranging from 0.01 to 1000 ppm, with a limit of detection (LOD) determined using the equation LOD = $(3.3 \times SD_{y\text{-intercept}})$/slope. Verification of calibration efficacy was conducted by analysis of a certified multi-anion reference standard, "VeriSpec Mixed Anion Standard 7", yielding percent recoveries from 91% to 99% for all seven anions.

Cations were analyzed utilizing an Optima 7300 DV Model Inductively Coupled Plasma – Optical Emission Spectrometer (ICP-OES, Perkin-Elmer, Waltham, MA) and using an Elemental Scientific 4DXC autosampler (Omaha, NE). Samples and standards were pumped into a nebulization spray chamber at a rate of 0.80 mL per minute. These aerosolized droplets of 10 μm in diameter were then drawn into the argon plasma via a gas pressure of 0.5 L per min. The carrier liquid was 1% trace metal grade nitric acid (HNO_3), and

a mixing T provided an inflow of 2.5 ppm Yttrium to serve as an internal standard. The argon plasma was generated using a gas flow rate of 14 L per min and a radio frequency inducement of 1350 W. Auxiliary gas flow was set to 0.2 L per min. Calibration standards were diluted from stock solutions certified by Spex, using deionized water prepared via a Labconco WaterPro DS system (Kansas City, MO) and trace metal grade nitric acid. Polypropylene flasks were used for all liquid preparations. Cations were calibrated using concentration ranging from 0.01 to 1000 ppm, with limit of detection (LOD) determined using the equation LOD = $(3.3 \times SD_{y\text{-intercept}})$/slope. Verification of calibration efficacy was conducted by analysis of a certified multi-anion reference standard (VWR, Radnor, PA), yielding percent recoveries ranging from 89% to 99% for all four cations.

2.9. Scanning electron microscopy

To determine if TPHP induced alterations to the yolk sac epithelium, a Hitachi Tabletop TM4000Plus Scanning Electron Microscope (SEM) was utilized to scan five independent locations on the yolk sac of each embryo. Prior to imaging, exposures were performed from 24 to 72 hpf within RO water, system water, or 2X EM containing 0.1% DMSO, 5 μM TPHP, 250 mM D-Mannitol, or 5 μM TPHP + 250 mM D-Mannitol. At 72 hpf, all embryos were fixed within 4% PFA as described above. Immediately before imaging, fixed embryos were flash frozen within a liquid nitrogen bath. Five different locations of the yolk sac of frozen embryos were then imaged using the following magnification and settings: 10 KV, setting 4, VSE, 2,000 X. Images were then analyzed within ImageJ (Version 1.8.0_172) using the following steps: 1) File → Open → Chose photo for analysis; 2) Choose *straight* line button on the toolbar and measure one side of the well to the other. Then chose Analyze → Set Scale (keep distance listed in pixels the same, make known distance 3, keep the pixel aspect ratio the same, Unit length is mm, and click the checkbox next to global); 3) Image → Adjust → Threshold (set first box to 0 and second box to 35) → click apply; 4) Analyze → Analyze particles (make sure the box next to summary is clicked); and 5) The number under total area provides the total area of microridges in the image, record and repeat steps.

2.10. Statistical analysis

For all data generated within this study, a general linear model (GLM) analysis of variance (ANOVA) ($\alpha = 0.05$) and Tukey-based multiple comparisons were performed using SPSS Statistics 24.

3. Results

3.1. TPHP does not affect embryonic sodium concentrations in situ

Relative to embryos exposed to vehicle (0.1% DMSO) from 24 to 72 hpf, exposure to TPHP (2.5 μM, 5 μM and 10 μM) from 24 to 72 hpf did not significantly affect sodium concentrations within the head, yolk sac, or trunk of embryonic zebrafish (Fig. 1). Pericardial area and yolk sac area were also quantified and, consistent with our prior studies, we found no significant differences in yolk sac area whereas TPHP increased pericardial area in a concentration-dependent manner (Fig. 1).

3.2. TPHP-induced pericardial edema is dependent on ionic strength of exposure media

To better characterize the ionic composition of exposure media used within this study, we first quantified the concentration (in ppm) of fluoride, chloride, nitrite, bromide, nitrate, phosphate, sulfate, sodium, calcium, potassium, or magnesium in RO Water, System Water, 0.5X EM, 1X EM, and 2X EM. Interestingly, the concentration of chloride increased as a function of EM strength and accounted for the majority of ions present within 0.5X, 1X, and 2X EM (Fig. 2; Figure S1). Indeed, the concentration of chloride within 2X EM was 3X higher than the next highest ion (sodium) (Fig. 2), a finding that was not surprising since three out of the four salts used to make EM contain chloride.

Embryos were exposed to 5 μM TPHP in different exposure media (RO Water, 0.5X EM, 1X EM, or 2X EM) from 24 to 72 hpf to determine if an increase in ionic strength of exposure media altered TPHP-induced pericardial edema. While TPHP decreased body length across all exposure media, TPHP did not affect yolk sac area within any of exposure media (Fig. 3). However, we found that, even in the presence of TPHP, pericardial area was not significantly different from water or vehicle controls when exposed within RO water or 0.5X EM (Fig. 3). However, when embryos were exposed to TPHP within 1X or 2X EM, pericardial area was significantly higher relative to water and vehicle controls, similar to what we have observed in this study and our prior studies using system water (Fig. 3). Interestingly, similar to our prior findings in system water, D-Mannitol completely mitigated TPHP-induced pericardial edema within co-exposed within 1X or 2X EM (Fig. 3).

To determine if a specific salt within EM was required for TPHP-induced pericardial edema, each EM ingredient was tested individually by exposing embryos to either vehicle (0.1% DMSO) or 5 μM TPHP. While there were no significant differences in body length or yolk sac area across all groups, pericardial area was significantly increased when embryos were exposed to TPHP within exposure media containing any of four EM ingredients (Fig. 4). Interestingly, the most significant effects were observed when embryos were exposed within exposure media containing KCl, $CaCl_2 \cdot 2H_2O$, or NaCl, suggesting that chloride may be playing a key role in pericardial edema formation.

3.3. D-Mannitol and ionic strength of exposure media do not impact TPHP uptake

Since D-mannitol (an osmotic diuretic) mitigates TPHP-induced pericardial edema and an increase in the ionic strength of exposure media exacerbates TPHP-induced pericardial edema, we quantified embryonic doses of TPHP and DPHP in the presence of D-mannitol or within RO Water vs. 2X EM. Interestingly, embryonic doses of TPHP and DPHP were not affected by the presence of D-mannitol nor significantly different within RO Water vs. 2X EM (Fig. 5), suggesting that differences in the severity of TPHP-induced pericardial edema under these varying experimental conditions were not attributed to differences in TPHP uptake.

3.4. TPHP disrupts the morphology and organization of the embryonic yolk sac epithelium

Within in Locations C and E, embryos exposed to TPHP within 2X EM exhibited extensive microridges relative to embryos exposed to vehicle (Fig. 6). While microridges in TPHP-

exposed embryos were higher at all locations, we only observed significant differences in those two locations. Embryos exposed to TPHP within 2X EM also exhibited extensive microridges relative to TPHP-exposed embryos in RO water at Locations C and E (Fig. 6). Interestingly, in all but one of the locations, embryos exposed to both TPHP and D-Mannitol within 2X EM had significantly less microridges compared to embryos exposed to TPHP alone (Fig. 6). Within all five locations, there was also an upward trend in the abundance of microridges observed within TPHP-exposed embryos, suggesting that an increase in ionic strength of exposure media exacerbated the generation of microridges within embryos.

4. Discussion

Based on our prior studies in developing zebrafish, TPHP is known to increase the number of ionocytes, as well as induce pericardial edema, liver enlargement and disrupt cardiac looping (Isales et al., 2015; McGee et al., 2013; Mitchell et al., 2018; Reddam et al., 2019; Wiegand et al., 2022). Within this study, we found that TPHP-induced pericardial edema is dependent on the presence of high ion concentrations within exposure media – a result that was likely associated with pericardial edema, increased ionocytes, and decreased body length found in our previous studies (Isales et al., 2015; McGee et al., 2013; Mitchell et al., 2018; Reddam et al., 2019; Wiegand et al., 2022; Yozzo et al., 2013). Numerous studies have shown how changing the ion concentration of media can impact embryonic development (Liao et al., 2009; Esaki M et al., 2009; Esbaugh et al., 2019). However, to our knowledge, little is known about how ionic strength of exposure media directly impacts the toxicity of chemicals within zebrafish embryos. Indeed, our findings have significant implications due to a lack of standardization of the ionic strength of exposure media within zebrafish embryo-based toxicity assays around the world.

To our knowledge, only one other study has investigated the potential impacts of contaminants on the skin epithelium of embryonic zebrafish. This study found that metal oxide nanoparticles caused skin damage on embryonic zebrafish, specifically cells found at the posterior fin and tail fin regions (Peng et al., 2018) but, unlike our study, most of the skin damage was localized to the posterior regions. Most studies in the published literature have investigated the epithelial layer of adult zebrafish rather than embryonic zebrafish. Interestingly, these studies have looked at the capacity for cutaneous wound healing within zebrafish (Naomi et al., 2021) and, as such, are difficult to compare to our results due to differences in the epithelial layer of adult vs. embryonic zebrafish. For example, embryonic zebrafish utilize the entire epithelial layer for osmoregulation due to the localization of ionocytes and aquaporins across their skin, while adult zebrafish have ionocytes and aquaporins localized to their gills, which occurs around 14 dpf (Breves et al., 2014; Dymowska et al., 2012; Evans, 2008, 2011; Gilmour, 2012; Hiroi and McCormick, 2012; Hwang and Lee, 2007; Hwang et al., 2011; Kumai and Perry, 2012; Wright and Wood, 2012). Embryonic zebrafish also do not develop scales until around 30 dpf (Le Guellec et al., 2003), making the embryonic skin more vulnerable to damage that may not impact adult zebrafish.

Interestingly, we found that an increase in ionic strength of exposure media exacerbated TPHP-induced generation of microridges within embryos. To our knowledge, we are

unaware of any other studies in the published literature that have 1) identified the potential for chemicals to induce an increase in the abundance of microridges in embryonic zebrafish and/or 2) discussed the potential functional role of increased microridges on the yolk sac epithelium. Found in many types of freshwater fish species, microridges provide rigidity and plasticity to surface epithelial cells; hydration of the apical surface; protection from pathogens and physical injury; retention of mucus; and storage of F-actin that can be utilized for wound healing (Apodaca and Gallo, 2013; Cone, 2009; Fishelson, 1984; Lam et al., 2015; Sharma et al., 2005; Sperry and Wassersug, 1976; Uehara et al., 1991). In zebrafish embryos, microridges are formed on multiple mucosal epithelial cells and are predominately localized on the outer layer of the embryo's epidermis, where their main purpose is to maintain glycans on the skin surface (Inaba et al., 2020). To our knowledge, there is little information available on the functional consequences of an increase or decrease in microridges. However, it's possible that an increase in microridges may play a role in wound repair and/or prevention of additional injury following exposure to chemicals (e.g., TPHP).

5. Conclusion

To our knowledge, this is the first study to investigate the potential impacts of TPHP on the embryonic yolk sac epithelium during early zebrafish development, and how changing ion composition of exposure media impacts the toxicity of TPHP within zebrafish embryos. Our data suggest that TPHP increases the frequency of microridges on the embryonic yolk sac epithelium, leading to potential impacts on osmoregulation during embryogenesis. We also found that changing the ionic strength of exposure media influenced the severity of pericardial edema formation, with increased ionic strength of the exposure media leading to increased pericardial edema. Finally, we demonstrated that D-Mannitol does not impact TPHP uptake in embryonic zebrafish while still preventing the formation of TPHP-induced pericardial edema.

Supplementary Material

Refer to Web version on PubMed Central for supplementary material.

Funding

Fellowship support was provided by the NRSA T32 Training Program (T32ES018827) to SAB. Research support was provided by a National Institutes of Health grant (R01ES027576) and USDA National Institute of Food and Agriculture Hatch Project (1009609) to DCV.

Data availability

Data will be made available on request.

References

Apodaca G, Gallo LI, 2013. Epithelial Polarity. 1(2), 1–115. 10.4199/C00077ED1V01Y201303BBC002.

Liao BK, Chen RD, Hwang PP, 2009. Expression regulation of Na+-K+-ATPase alpha1-subunit subtypes in zebrafish gill ionocytes. Am. J. Physiol. Regul. Integr. Comp. Physiol 296 (6) 10.1152/AJPREGU.00029.2009.

Brand M, Granato M, Nusslein-Volhard C, 2002. Zebrafish: A Practical Approach (Practical Approach Series, 261). In: Nuslein-Volhard C, Dahm R (Eds.). Oxford University Press.

Breves JP, McCormick SD, Karlstrom RO, 2014. Prolactin and teleost ionocytes: new insights into cellular and molecular targets of prolactin in vertebrate epithelia. Gen. Comp. Endocrinol 21. 10.1016/J.YGCEN.2013.12.014.

Brotzmann K, Escher SE, Walker Paul, Braunbeck T, 2022. Potential of the zebrafish (Danio rerio) embryo test to discriminate between chemicals of similar molecular structure-a study with valproic acid and 14 of its analogues. Archives of Toxicology, 96, 3033–3051. 10.1007/s00204-022-03340-z. [PubMed: 35920856]

Chen Y, Ren C, Ouyang S, Hu X, Zhou Q, 2015. Mitigation in Multiple Effects of Graphene Oxide Toxicity in Zebrafish Embryogenesis Driven by Humic Acid. Environ. Sci. Tech 49 (16), 10147–10154. 10.1021/ACS.EST.5B02220.

Choi SA, Park CS, Kwon OS, Giong HK, Lee JS, Ha TH, Lee CS, 2016. Structural effects of naphthalimide-based fluorescent sensor for hydrogen sulfide and imaging in live zebrafish. Sci. Rep 6 10.1038/SREP26203.

Cindrova-Davies T, Jauniaux E, Elliot MG, Gong S, Burton GJ, Charnock-Jones DS, 2017. RNA-seq reveals conservation of function among the yolk sacs of human, mouse, and chicken. Proceedings of the National Academy of Sciences of the United States of America, 114(24), E4753–E4761. 10.1073/PNAS.1702560114. [PubMed: 28559354]

Cone RA, 2009. Barrier properties of mucus. Adv. Drug Deliv. Rev 61 (2), 75–85. 10.1016/J.ADDR.2008.09.008. [PubMed: 19135107]

Dolgova NV, Hackett MJ, MacDonald TC, Nehzati S, James AK, Krone PH, George GN, Pickering IJ, 2016. Distribution of selenium in zebrafish larvae after exposure to organic and inorganic selenium forms. Metallomics : Integrated Biometal Science 8 (3), 305–312. 10.1039/C5MT00279F. [PubMed: 26781816]

Duan J, Yu Y, Shi H, Tian L, Guo C, Huang P, Zhou X, Peng S, Sun Z, 2013. Toxic Effects of Silica Nanoparticles on Zebrafish Embryos and Larvae. PLoS One 8 (9), e74606. [PubMed: 24058598]

Dymowska AK, Hwang PP, Goss GG, 2012. Structure and function of ionocytes in the freshwater fish gill. Respir. Physiol. Neurobiol 184 (3), 282–292. 10.1016/J.RESP.2012.08.025. [PubMed: 22981968]

Esaki M, Hoshijima K, Nakamura N, et al. , 2009. Mechanism of Development of Ionocytes Rich in Vacuolar-Type H(+)-ATPase in the Skin of Zebrafish Larvae. Dev. Biol 329 (1), 116–129. 10.1016/j.ydbio.2009.02.026. [PubMed: 19268451]

Esbaugh AJ, Brix KV, Grosell M, 2019. Na+ K+ ATPase isoform switching in zebrafish during transition to dilute freshwater habitats. Proc. R. Soc. B 286 (1903). 10.1098/RSPB.2019.0630..

Evans D, 2008. Teleost fish osmoregulation: What have we learned since August Krogh, Homer Smith, and Ancel Keys. Am. J. Physiol. Regul. Integr. Comp. Physiol 295 (2) 10.1152/AJPREGU.90337.2008/SUPPL_FILE/DESCRIPTIONS.DOCX.

Evans D, 2011. Freshwater Fish Gill Ion Transport: August Krogh to morpholinos and microprobes. Acta Physiol. 202 (3), 349–359. 10.1111/J.1748-1716.2010.02186.X.

Fishelson L, 1984. A comparative study of ridge-mazes on surface epithelial cell-membranes of fish scales (Pisces, Teleostei). Zoomorphology 104 (4), 231–238. 10.1007/BF00312036/METRICS.

Fridman S, 2020. Ontogeny of the Osmoregulatory Capacity of Teleosts and the Role of Ionocytes. Front. Mar. Sci 10.3389/fmars.2020.00709.

Ge C, Lu W, Chen A, 2017. Quantitative proteomic reveals the dynamic of protein profile during final oocyte maturation in zebrafish. Biochem. Biophys. Res. Commun 490 (3), 657–663. 10.1016/J.BBRC.2017.06.093. [PubMed: 28634081]

Gilmour KM, 2012. New insights into the many functions of carbonic anhydrase in fish gills. Respir. Physiol. Neurobiol 184 (3), 223–230. 10.1016/J.RESP.2012.06.001. [PubMed: 22706265]

Guh YJ, Lin CH, Hwang PP, 2015a. Osmoregulation in zebrafish: ion transport mechanisms and functional regulation. EXCLI Journal, 14, 627. 10.17179/EXCLI2015-246. [PubMed: 26600749]

Guh YJ, Lin CH, Hwang PP, 2015b. Osmoregulation in zebrafish: Ion transport mechanisms and functional regulation. EXCLI J. 14, 627–659. 10.17179/excli2015-246. [PubMed: 26600749]

Hagedorn M, Kleinhans FW, Artemov D, Pilatus U, 1998. Characterization of a Major Permeability Barrier in the Zebrafish Embryo. Biol. Reprod 59 (5), 1240–1250. 10.1095/BIOLREPROD59.5.1240. [PubMed: 9780333]

Hermsen SAB, van den Brandhof EJ, van der Ven LTM, Piersma AH, 2017. Relative embryotoxicity of two classes of chemicals in a modified zebrafish embryotoxicity test and comparison with their in vivo potencies. Toxicol. In Vitro 25 (3), 745–753. 10.1016/J.TIV.2011.01.005.

Hill A, Bello S, Prasch A, Peterson R, Heideman W, 2004. Water permeability and TCDD-induced edema in zebrafish early-life stages. Toxicol. Sci.: Off. J. Soc. Toxicol 78 (1), 78–87. 10.1093/TOXSCI/KFH056.

Hiroi J, McCormick SD, 2012. New insights into gill ionocyte and ion transporter function in euryhaline and diadromous fish. Respir. Physiol. Neurobiol 184 (3), 257–268. 10.1016/J.RESP.2012.07.019. [PubMed: 22850177]

Hwang P, Lee TH, 2007. New insights into fish ion regulation and mitochondrion-rich cells. In: Comparative Biochemistry and Physiology - A Molecular and Integrative Physiology, Vol. 148, Issue 3, Pergamon, pp. 479–497, 10.1016/j.cbpa.2007.06.416. [PubMed: 17689996]

Hwang P, Chou MY, 2013. Zebrafish as an animal model to study ion homeostasis. Pflugers Arch. 465 (9), 1233–1247. 10.1007/S00424-013-1269-1. [PubMed: 23568368]

Hwang P, Lee TH, Lin LY, 2011. Ion regulation in fish gills: Recent progress in the cellular and molecular mechanisms. Am. J. Physiol. - Regulatory Integrative Comparative Physiol 10.1152/ajpregu.00047.2011.

Inaba Y, Chauhan V, van Loon AP, Choudhury LS, Sagasti A, 2020. Keratins and the plakin family cytolinker proteins control the length of epithelial microridge protrusions. Elife 9, 1–27. 10.7554/ELIFE.58149.

Isales GM, Hipszer RA, Raftery TD, Chen A, Stapleton HM, Volz DC, 2015. Triphenyl phosphate-induced developmental toxicity in zebrafish: Potential role of the retinoic acid receptor. Aquat. Toxicol 161, 221–230. 10.1016/j.aquatox.2015.02.009. [PubMed: 25725299]

Kumai Y, Perry SF, 2012. Mechanisms and regulation of Na+ uptake by freshwater fish. Respir. Physiol. Neurobiol 184 (3), 249–256. 10.1016/J.RESP.2012.06.009. [PubMed: 22698881]

Kwong RWM, Kumai Y, Perry SF, 2014. The physiology of fish at low pH: the zebrafish as a model system. J. Exp. Biol 217 (5), 651–662. 10.1242/JEB.091603. [PubMed: 24574381]

Kwong RWM, Kumai Y, Perry SF, 2016. Neuroendocrine control of ionic balance in zebrafish. Gen. Comp. Endocrinol 234, 40–46. 10.1016/J.YGCEN.2016.05.016. [PubMed: 27179885]

Kwong RWM, Perry SF, 2015. An essential role for parathyroid hormone in gill formation and differentiation of ion-transporting cells in developing zebrafish. Endocrinology 156 (7), 2384–2394. 10.1210/en.2014-1968. [PubMed: 25872007]

Lam PY, Mangos S, Green JM, Reiser J, Huttenlocher A, 2015. In Vivo Imaging and Characterization of Actin Microridges. PLoS One 10 (1), e0115639. 10.1371/journal.pone.0115639. [PubMed: 25629723]

Le Guellec D, Morvan-Dubois G, Sire JY, 2003. Skin development in bony fish with particular emphasis on collagen deposition in the dermis of the zebrafish (Danio rerio). Int. J. Dev. Biol 48 (2–3), 217–231. 10.1387/IJDB.15272388.

Li Q, Frank M, Thisse CI, Thisse BV, Uitto J, 2011. Zebrafish: A Model System to Study Heritable Skin Diseases. J, Invest. Dermatol 131 (3), 565–571. 10.1038/JID.2010.388. [PubMed: 21191402]

Link V, Shevchenko A, Heisenberg CP, 2006. Proteomics of early zebrafish embryos. BMC Dev. Biol 6. 10.1186/1471-213X-6-1.

McCollum CW, Conde-Vancells J, Hans C, Vazquez-Chantada M, Kleinstreuer N, Tal T, Knudsen T, Shah SS, Merchant FA, Finnell RH, Gustafsson JÅ, Cabrera R, Bondesson M, 2017. Identification of vascular disruptor compounds by analysis in zebrafish embryos and mouse embryonic endothelial cells. Reprod. Toxicol 70, 60–69. 10.1016/J.REPROTOX.2016.11.005. [PubMed: 27838387]

Mccollum CW, Ducharme NA, Bondesson M, Gustafsson JA, 2011. Developmental toxicity screening in zebrafish. Birth Defects Res. C Embryo Today 93 (2), 67–114. 10.1002/BDRC.20210. [PubMed: 21671351]

McGee SP, Cooper EM, Stapleton HM, Volz DC, 2012. Early zebrafish embryogenesis is susceptible to developmental TDCPP exposure. Environ. Health Perspect 120 (11), 1585–1591. 10.1289/EHP.1205316. [PubMed: 23017583]

McGee SP, Konstantinov A, Stapleton HM, Volz DC, 2013. Aryl phosphate esters within a major pentaBDE replacement product induce cardiotoxicity in developing zebrafish embryos: Potential role of the aryl hydrocarbon receptor. Toxicol. Sci 133 (1), 144–156. 10.1093/toxsci/kft020. [PubMed: 23377616]

McGruer V, Tanabe P, Vliet SMF, Dasgupta S, Qian L, Volz DC, Schlenk D, 2021. Effects of Phenanthrene Exposure on Cholesterol Homeostasis and Cardiotoxicity in Zebrafish Embryos. Environ. Toxicol. Chem 40 (6), 1586–1595. 10.1002/ETC.5002. [PubMed: 33523501]

Mitchell CA, Dasgupta S, Zhang S, Stapleton HM, Volz DC, 2018. Disruption of nuclear receptor signaling alters triphenyl phosphate-induced cardiotoxicity in zebrafish embryos. Toxicol. Sci 163 (1), 307–318. 10.1093/toxsci/kfy037. [PubMed: 29529285]

Mitchell CA, Reddam A, Dasgupta S, Zhang S, Stapleton HM, Volz DC, 2019. Diphenyl Phosphate-Induced Toxicity during Embryonic Development. Environ. Sci. Tech 53 (7), 3908–3916. 10.1021/acs.est.8b07238.

Naomi R, Bahari H, Yazid MD, Embong H, Othman F, 2021. Zebrafish as a Model System to Study the Mechanism of Cutaneous Wound Healing and Drug Discovery: Advantages and Challenges. Pharmaceuticals 14 (10), 1058. 10.3390/PH14101058. [PubMed: 34681282]

Narumanchi S, Wang H, Perttunen S, Tikkanen I, Lakkisto P, Paavola J, 2021. Zebrafish Heart Failure Models. Front. Cell Dev. Biol 9, 1061. 10.3389/FCELL.2021.662583/XML/NLM.

Pelster B, Burggren WW, 1996. Disruption of hemoglobin oxygen transport does not impact oxygen-dependent physiological processes in developing embryos of zebra fish (Danio rerio). Circ. Res 79 (2), 358–362. 10.1161/01.RES.79.2.358. [PubMed: 8756015]

Peng G, He Y, Zhao M, Yu T, Qin Y, Lin S, 2018. Differential effects of metal oxide nanoparticles on zebrafish embryos and developing larvae. Environ. Sci. Nano 5 (5), 1200–1207. 10.1039/C8EN00190A.

Reddam A, Mitchell CA, Dasgupta S, Kirkwood JS, Vollaro A, Hur M, Volz DC, 2019. mRNA-Sequencing Identifies Liver as a Potential Target Organ for Triphenyl Phosphate in Embryonic Zebrafish. Toxicol. Sci 10.1093/toxsci/kfz169.

Rombough P, 2007. The functional ontogeny of the teleost gill: Which comes first, gas or ion exchange? Comp. Biochem. Physiol. A Mol. Integr. Physiol 148 (4), 732–742. 10.1016/J.CBPA.2007.03.007. [PubMed: 17451987]

Sant KE, Timme-Laragy AR, 2018. Zebrafish as a Model for Toxicological Perturbation of Yolk and Nutrition in the Early Embryo. Curr. Environ. Health Rep 5 (1), 125–133. 10.1007/S40572-018-0183-2. [PubMed: 29417450]

Serluca FC, Drummond IA, Fishman MC, 2002. Endothelial signaling in kidney morphogenesis: A role for hemodynamic forces. Curr. Biol 12 (6), 492–497. 10.1016/S0960-9822(02)00694-2/ATTACHMENT/5BA67E49-4807-453E-8B8B-087457139F67/MMC1.PDF. [PubMed: 11909536]

Sharma A, Anderson KI, Müller DJ, 2005. Actin microridges characterized by laser scanning confocal and atomic force microscopy. FEBS Lett. 579 (9), 2001–2008. 10.1016/J.FEBSLET.2005.02.049. [PubMed: 15792810]

Souder JP, Gorelick DA, 2017. Quantification of Estradiol Uptake in Zebrafish Embryos and Larvae. Toxicol. Sci.: Off. J. Soc. Toxicol 158 (2), 465–474. 10.1093/TOXSCI/KFX107.

Sperry DG, Wassersug RJ, 1976. A proposed function for microridges on epithelial cells. Anat. Rec 185 (2), 253–257. 10.1002/AR.1091850212. [PubMed: 1275311]

Uehara K, Miyoshi M, Miyoshi S, 1991. Cytoskeleton in microridges of the oral mucosal epithelium in the carp, Cyprinus carpio. The Anatomical Record 230 (2), 164–168. 10.1002/AR.1092300203. [PubMed: 1714256]

Von Hellfeld R, Brotzmann K, Baumann L, Strecker R, Braunbeck T, 2020. Adverse effects in the fish embryo acute toxicity (FET) test: a catalogue of unspecific morphological changes versus more specific effects in zebrafish (Danio rerio) embryos. Environ. Sci. Eur 32, 122. 10.1186/s12302-020-00398-3.

Wiegand J, Cheng V, Reddam A, Avila-Barnard S, Volz DC, 2022. Triphenyl phosphate-induced pericardial edema is associated with elevated epidermal ionocytes within zebrafish embryos. Environ. Toxicol. Pharmacol 89, 103776 10.1016/J.ETAP.2021.103776. [PubMed: 34798236]

Wright PA, Wood CM, 2012. Seven things fish know about ammonia and we don't. Respir. Physiol. Neurobiol 184 (3), 231–240. 10.1016/J.RESP.2012.07.003. [PubMed: 22910326]

Yozzo K, Isales G, Rafferty, Volz D, 2013a. High-content screening assay for identification of chemicals impacting cardiovascular function in zebrafish embryos. Environm. Scie. Technol 47 (19), 11302–11310. 10.1021/ES403360Y.

Yozzo KL, McGee SP, Volz DC, 2013b. Adverse outcome pathways during zebrafish embryogenesis: A case study with paraoxon. Aquat. Toxicol 126, 346–354. 10.1016/J.AQUATOX.2012.09.008. [PubMed: 23046524]

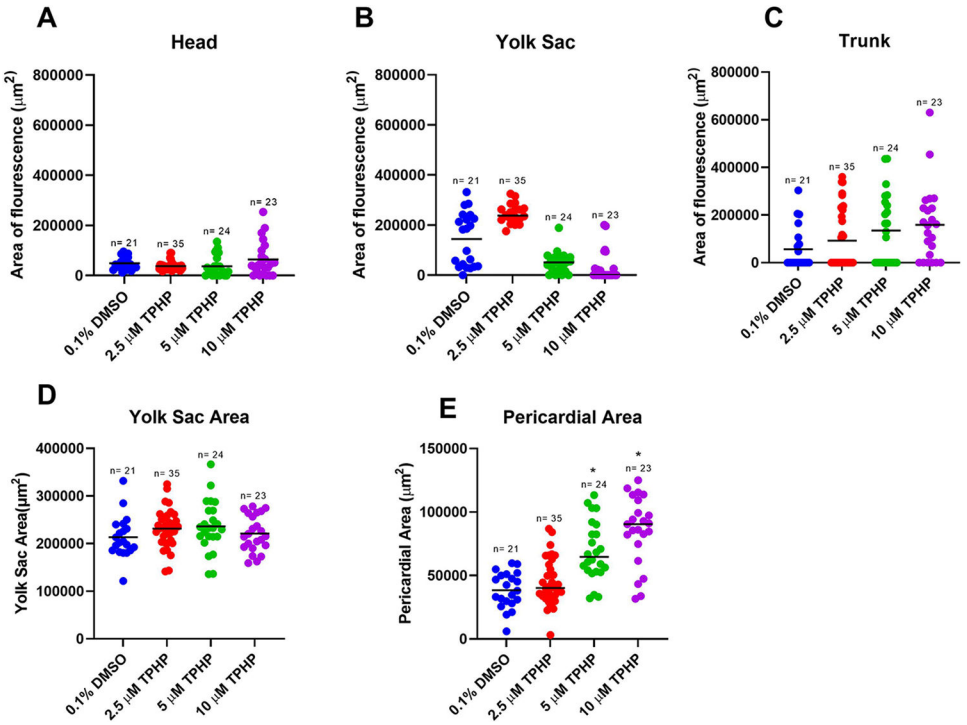

Fig. 1.

Mean (±standard deviation) of the area of CoroNa Green AM fluorescence in the head (A), yolk sac (B), trunk (C), total area of the yolk sac (D), and pericardial area (E) of embryos exposed to vehicle (0.1% DMSO), 2.5 μM TPHP, 5 μM TPHP or 10 μM TPHP from 24 to 72 hpf. Asterisk (*) denotes a significant difference ($p < 0.05$) relative to vehicle controls.

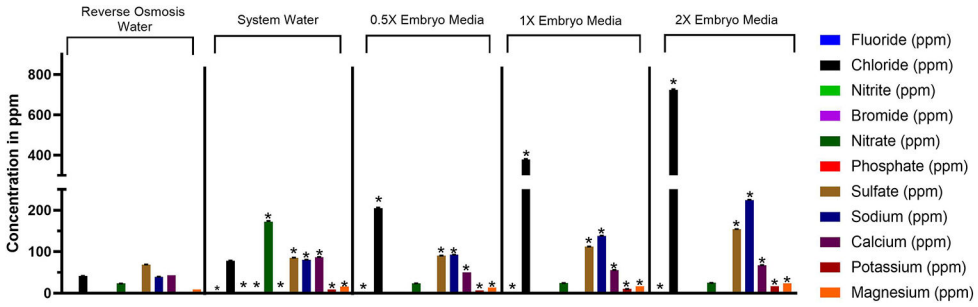

Fig. 2.

Mean (±standard deviation) concentration (in ppm) of fluoride, chloride, nitrite, bromide, nitrate, phosphate, sulfate, sodium, calcium, potassium, or magnesium in Reverse Osmosis (RO) Water, System Water, 0.5X Embryo Media (EM), 1X EM, and 2X EM. Asterisk (*) denotes a significant difference ($p < 0.05$) relative to RO water.

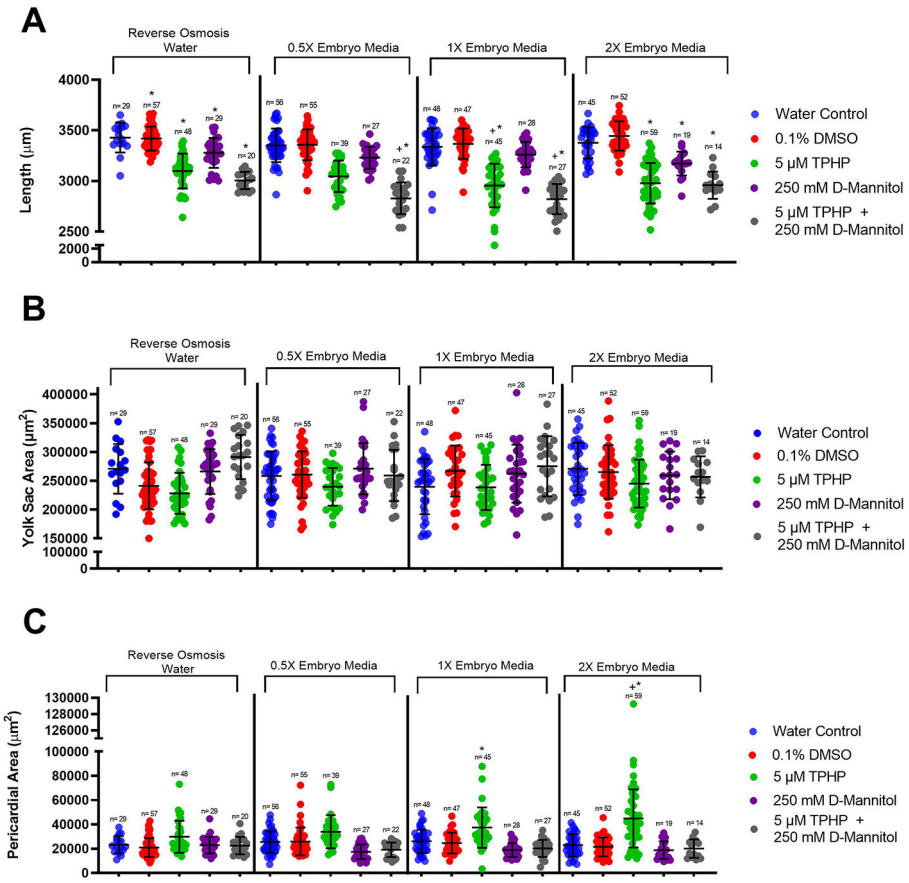

Fig. 3.

Mean (±standard deviation) of length (A), yolk sac area (B) and pericardial area (C) of embryos exposed to water control, vehicle (0.1% DMSO), 5 μM TPHP, 250 mM D-Mannitol, or 5 μM TPHP + 250 mM D-Mannitol in different types of media – Reverse Osmosis (RO) Water, 0.5X Embryo Media (EM), 1X EM, or 2X EM. Plus sign (+) denotes a significant difference ($p < 0.05$) relative to 5 μM TPHP in RO water, whereas asterisk (*) denotes a significant difference ($p < 0.05$) relative to embryos exposed to vehicle (0.1% DMSO) within the same exposure medium (RO Water, 0.5X EM, 1X EM or 2X EM).

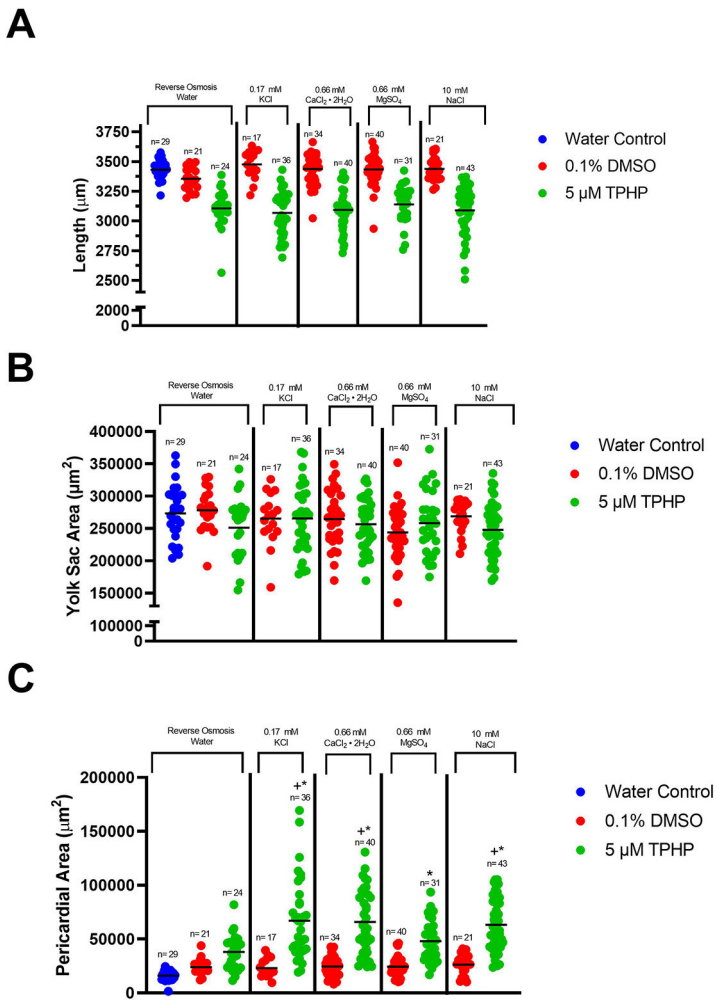

Fig. 4.

Mean (±standard deviation) of length (A), yolk sac area (B), and pericardial area (C) of embryos exposed to water control, vehicle (0.1% DMSO) or 5 µM TPHP in varying exposure media (10.18 mM KCl, 19.73 mM $CaCl_2{\cdot}2H_2O$, 40.71 mM $MgSO_4$, and 294.3 mM NaCl). Asterisk (*) denotes a significant difference ($p < 0.05$) relative to vehicle (0.1% DMSO) in the same exposure medium (0.17 mM KCl, 0.66 mM $CaCl_2{\cdot}2H_2O$, 0.66 mM $MgSO_4$, and 10 mM NaCl), whereas plus sign (+) denotes a significant difference ($p < 0.05$) relative to embryos exposed to 5 µM TPHP in Reverse Osmosis (RO) Water.

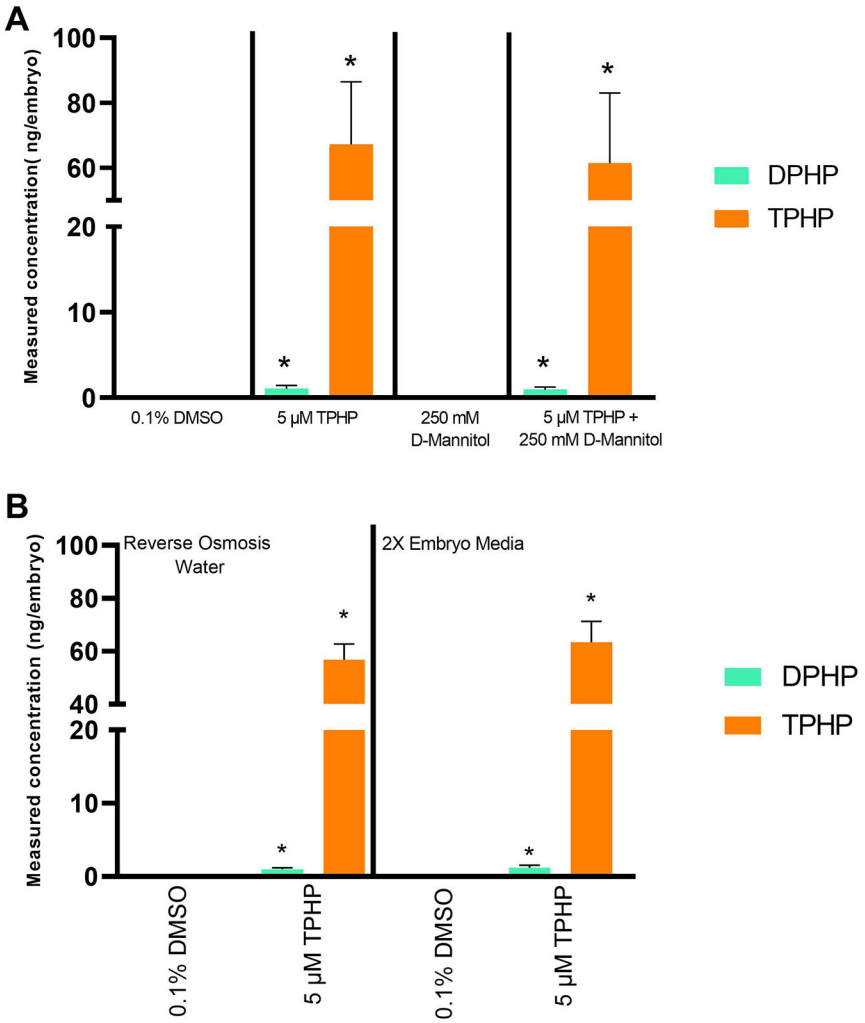

Fig. 5.

A) Mean (±standard deviation) of measured concentration of DPHP and TPHP (ng/embryo) in embryos exposed to vehicle (0.1% DMSO), 5 µM TPHP, 250 mM D-Mannitol, and 5 µM TPHP + 250 mM D-Mannitol from 24 to 72 hpf. Asterisk (*) denotes a significant difference ($p < 0.05$) relative to vehicle (0.1% DMSO). B) Mean (±standard deviation) of measured concentration of DPHP and TPHP (ng/embryo) in embryos exposed to vehicle (0.1% DMSO) or 5 µM TPHP in different exposure media – Reverse Osmosis (RO) Water or 2X Embryo Media (EM). Asterisk (*) denotes a significant difference ($p < 0.05$) relative to vehicle (0.1% DMSO).

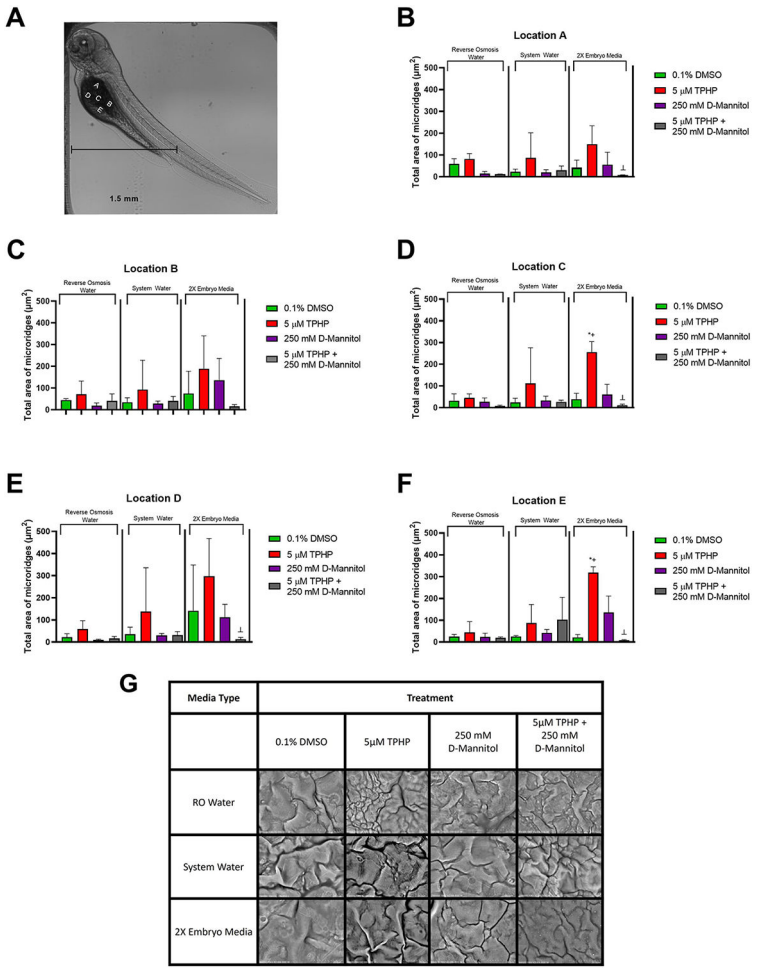

Fig. 6.

Locations (A, B, C, D, and E) used for SEM on the yolk sac of embryonic zebrafish (A). Panels B-F show the total area of microridges across treatment groups within each location. (G) Representative images of Location C are shown. Asterisk (*) denotes a significant difference ($p < 0.05$) relative to vehicle (0.1% DMSO) within the same exposure medium. Plus sign (+) denotes a significant difference ($p < 0.05$) relative to 5 μM TPHP in Reverse Osmosis (RO) Water. Upside-down T (⊥) denotes a significant difference ($p < 0.05$) relative to 5 μM TPHP in 2X Embryo Media (EM). Within all five locations, there was an increase in the abundance of microridges found in TPHP-exposed embryos, suggesting that, in the presence of TPHP, an increase in ionic strength of exposure media is associated with the formation of microridges within embryos.